"Snowing" Graphene using Microwave Ovens

Yangyong Sun, Liangwei Yang, Kailun Xia, Haizhou Liu, Dong Han, Yingying Zhang, and Jin Zhang**

Developing a simple and industrially scalable method to produce graphene with high quality and low cost will determine graphene's future. The two conventional approaches, chemical vapor deposition and liquid-phase exfoliation, require either costly substrates with limited production rate or complicated post treatment with limited quality, astricting their development. Herein, an extremely simple process is presented for synthesizing high quality graphene at low-cost in the gas phase, similar to "snowing," which is catalyst-free, substrate-free, and scalable. This is achieved by utilizing corona discharge of SiO_2/Si in an ordinary household microwave oven at ambient pressure. High quality graphene flakes can "snow" on any substrate, with thin-flakes even down to the monolayer. In particular, a high yield of≈6.28% or a rate of up to ≈0.11 g h^{-1} can be achieved in a conventional microwave oven. It is demonstrated that the snowing process produces foam-like, fluffy, 3D macroscopic architectures, which are further used in strain sensors for achieving high sensitivity (average gauge factor ≈ 171.06) and large workable strain range (0%–110%) simultaneously. It is foreseen that this facile and scalable strategy can be extended for "snowing" other functional 2D materials, benefiting their low-cost production and wide applications.

Snowing, a natural phenomenon, is a falling down process of ice crystals formed by deposition of H_2O molecules on condensation nuclei from the atmosphere. Self-assembly snowflakes can form into white and fluffy snowfield. The planar high quality snow crystals are similar to 2D nanomaterials, such as graphene, etc. It would be fantastic if a scalable snowing process of graphene with high quality and low cost could be realized,[1–3] allowing solution-free, catalyst-free, and substrate-free graphene products to be obtained directly. More than several decades after exfoliating graphite in agitated fluids to produce graphene oxide by Hummers' method,[4] significant efforts have been directed toward scalable production of graphene.[5–10] Liquid-phase exfoliation (LPE) can yield kilograms of graphene with low cost, but requires suitable solvents, proper additional surfactants, and complicated post treatments to purify and stabilize the suspension. This inevitably brings about low quality and contamination of graphene.[11,12] Conversely, chemical vapor deposition (CVD) is another choice, assisted by metal catalysts or other aids at high temperature. CVD is good for surface devices and can realize roll-to-roll preparation of high quality graphene film, but is limited by large consumption of metal foils and energy, complex craftsmanship, and the transfer process.[13–15] Both LPE and CVD have their own pros and cons, it seems that "snowing" graphene can give us a whole new space to explore. In the last decades, microwave plasma reactors[16] and DC arc discharge[17] are proven to be substrate-free methods for syntheses of carbon nanomaterials including graphene of high quality, but complex and costly equipment as well as low pressure are always required.[18,19] Therefore, how to develop a facile scalable technology of producing high quality graphene with low cost, especially "snowing" graphene, still remains challenge. Besides, the soft snowflakes can self-assemble in a snowfield. The snowfield is very fluffy, similar to lamellar coral in the ocean which can disperse strain derived from tidal forces. Such a structure may contribute to some applications such as sensors,[20,21] etc. So, rational assembly of graphene sheets into macroscopic architectures should also be considered for applications.[22–24] Macroscopic architectures with different functions can exhibit different performance. Orderly and densely stacked structures such as graphene fiber or film can be realized by dimension-confined strategies[25] or filtration assembly[26] of graphene due to strong π–π interactions between planar graphene sheets. This will contribute to good mechanical flexibility and strength for actuator.[27] Alternatively, a 3D assembled framework from graphene sheets can be obtained by hydrothermal or freezing-drying through π-conjugation, giving great enhancement of surface/interface interaction and mutability for electrochemical and electromechanical devices.[28]

Y. Y. Sun, L. W. Yang, Prof. J. Zhang
Center for Nanochemistry
Beijing Science and Engineering Center for Nanocarbons
Beijing National Laboratory for Molecular Sciences
College of Chemistry and Molecular Engineering
Peking University
Beijing 100871, China
E-mail: jinzhang@pku.edu.cn
K. L. Xia, Prof. Y. Y. Zhang
Department of Chemistry and Center for Nano and Micro Mechanics (CNMM)
Tsinghua University
Beijing 100084, China
E-mail: yingyingzhang@tsinghua.edu.cn
H. Z. Liu, D. Han, Prof. J. Zhang
Division of Powder Graphene Technology
Beijing Graphene Institute
Beijing 100095, China
The ORCID identification number(s) for the author(s) of this article can be found under https://doi.org/10.1002/adma.201803189.

DOI: 10.1002/adma.201803189

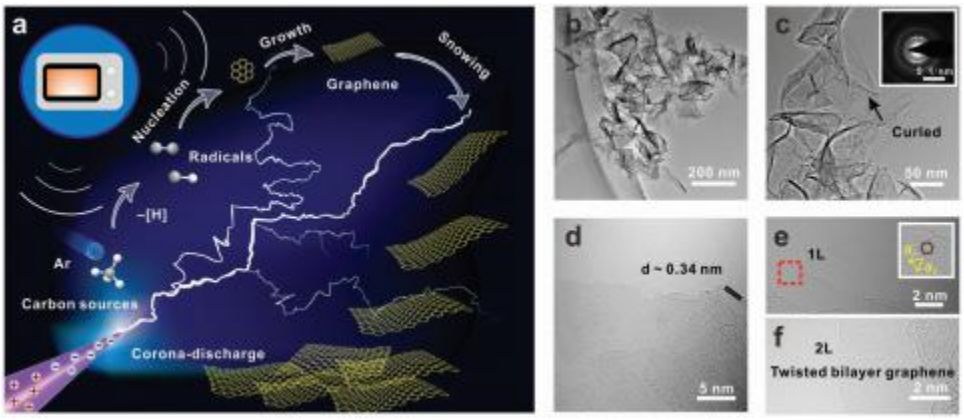

Figure 1. Schematic illustration and basic characterization of snowing graphene using microwave ovens. a) Schematic illustration of growing GS using a conventional microwave oven. Corona discharge can be generated to promote snowing graphene in the gas phase. b,c) Low-magnification TEM image and selected-area electron diffraction pattern (as an inset) of GS. d–f) Low-voltage, aberration-corrected, high-resolution TEM image of GS layers and the edges of single layer and two layers. An enlarged area derived from the red box in inset (e) is shown as an inset, exhibiting the sixfold symmetry.

Herein, we demonstrate a snowing process for scalable preparation of graphene flakes. Like the process of H_2O molecules nucleation and then growth in the atmosphere, the carbon sources can nucleate and grow in the gas phase and then floating with the gas flow. This was realized by a simple and low-cost corona discharge of SiO_2/Si in an ordinary household microwave oven at ambient pressure, which is facile and low-cost. Large quantities of graphene flakes can snow directly in the gas phase without the assistance of catalyst or substrate. The yield can be ≈6.28% and a rate can be up to ≈0.11 g h^{-1}. The derived graphene exhibits high quality of the D/G ≈ 0.36, an average size of ≈100 ± 16 nm and ≈74.4% of the layers being five layers or less. Similar to snowing snowflakes into snowfield, the "Graphene Snow" (GS) can self-assemble into fluffy and foam-like macroscopic architectures, exhibiting high sensitivity (average gauge factor ≈ 171.06) as well as large workable strain range (0%–110%) when applied to strain sensors. In addition, close stacking macroscopic architectures of GS patterns can be obtained by inkjet printing, producing good conductivity and mechanical properties. Compared to conventional methods of graphene preparation, this work demonstrates a simple and scalable method for producing graphene and other 2D materials, and a way to assemble microscopic architectures into macroscopic architectures, with likely applications in sensors and printed electronics, etc.

The experiment was carried out in an ordinary household microwave oven, within a quartz tube passing through the interior. A corona discharge of SiO_2/Si was generated inside the quartz tube, producing high quality graphene sheets within seconds. Note that instead of SiO_2/Si, other conductive materials such as fresh metal wires, foils, and syringe needles, and so on, can also be employed (Figure S1, Supporting Information). As shown in the video, SiO_2/Si was discharging in the quartz tube (Video, Supporting Information), which we attribute to charge accumulation around the tips at the edges of SiO_2/Si.[29] The temperature of the quartz tube detected by a hand-held thermometer can reach 710 °C in about 4 min from room temperature, which we think is lower than the temperature of the plasma (Figure S2, Supporting Information). By introducing methane into the system, graphene sheets can be produced directly in the gas phase and then floating with the gas flow, which is similar to snowing (**Figure 1**a). The whole process can be realized within 4 min, and no substrate or catalyst is required. The corona discharge triggered graphene snow can snow on different substrates (Figure S3, Supporting Information) and various carbon sources can be used to produce GS (Figures S4 and S5, Supporting Information). Typical low-magnification transmission electron microscopy (TEM) images of GS are shown in Figure 1b and Figure S6 (Supporting Information), in which the GS is flaky. Some boundaries of GS are folded, as shown in Figure 1c and Figure S7 (Supporting Information), enlarged TEM images. Selected area electron diffraction (SAED) in Figure 1c reveals that GS flake is of high quality. Low-voltage, aberration-corrected, high-resolution TEM was used to characterize GS, and we observed an interlayer spacing of ≈0.34 nm (Figure 1d; Figure S8, Supporting Information). Also, GS exhibits the sixfold symmetry, indicating its structural integrity (Figure 1e,f).

Raman spectroscopy has been proved to be an effective way for testing and probing local structural information in graphene.[30] As seen in **Figure 2**a, the peaks at about 1343, 1570, and 2682 cm^{-1} can be attributed to the D, G, and 2D bands, respectively.[30] Compared with reduced graphene oxide (RGO) and graphene oxide (GO), GS exhibits a better quality, which can be clearly observed from the low intensity ratio of I_D/I_G. Note that the D peak of GS shows that there may exist some grain boundaries of graphene. Also, I_D/I_G increases with the methane flux, indicating that a smaller methane flux produces a higher quality of GS (Figure S9, Supporting Information). In addition, X-ray photoelectronspectroscopy (XPS) of graphene reveals that the ratio of C/O is around 41.8, revealing extremely low oxygen content (Figure S10, supporting Information), close to the value measured in graphite (C/O ≈ 46.62),[31] but much superior to RGO (C/O < 17)[32,33] (Table S1, Supporting Information). A predominant sp^2 carbon peak (284.8 eV), a C–H peak (285.2 eV), as well as a broad C–O peak and shake-up peak can be observed in the XPS C 1s spectrum in Figure 2b, revealing the featured signals of our good quality GS.[34] GS was

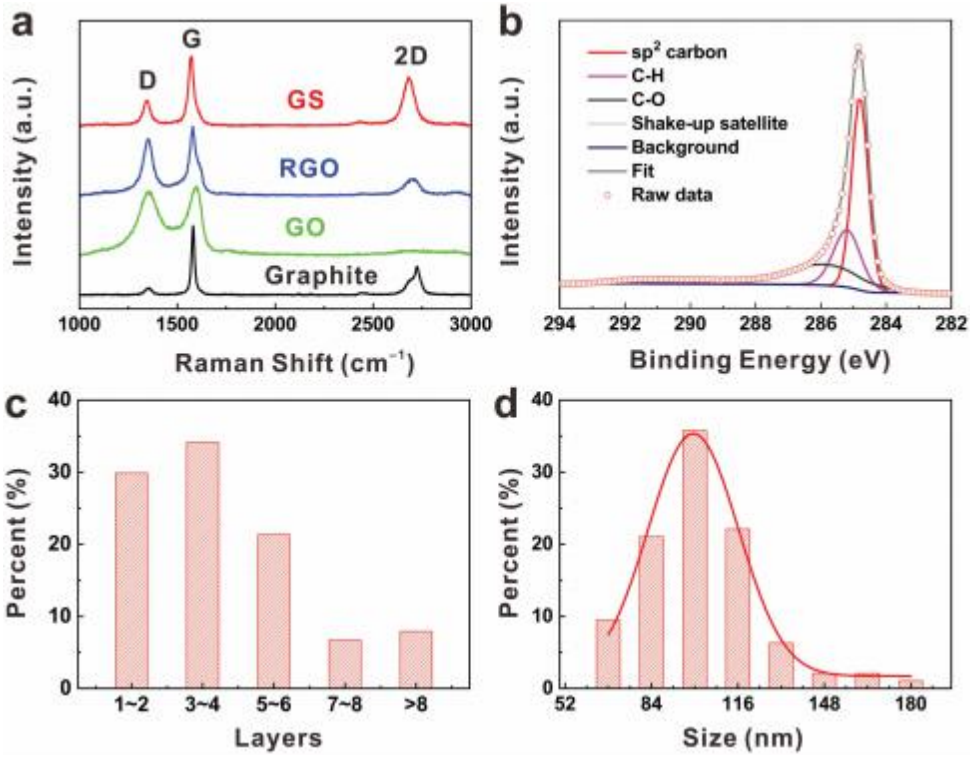

Figure 2. Characterizations and analysis of high-quality GS. a) Raman spectra of GS, RGO, GO, and graphite, showing that GS is of high quality. b) C1s states of GS produced by a microwave oven. c) Layer and d) size distribution of GS at a low CH_4 concentration of 1.0 vol%.

further confirmed by X-ray diffraction (XRD). As can be seen an inconspicuous peak at about 26° in contrast with graphite can be indexed to (002) of graphene (JCPDS card 41–1487),[35] while the weak intensity indicates its lack of layered periodic structures of graphite (Figure S11, supporting Information).[36] When a low CH_4 concentration of 1.0 vol% was input into the system, statistics suggest that ≈74.4% of the sheets of GS are five layers or less (Figure 2c), together with a distribution in average size of 100 ± 16 nm (Figure 2d). Increasing the methane flux can lead to an increase in the number of layers of GS (Figure S12, Supporting Information). The estimated yield of GS flakes can be up to ≈6.28% (the *g*/*g* weight ratio of graphene/carbon sources) when inputting 14.34 mg CH_4 per minute (Figure S13, Supporting Information). The rate can be up to ≈0.11 g h^{-1} when a methane flux of 100 sccm was introduced, comparable with those of RGO[37] and LPE graphene[38] (Table S2, Supporting Information).

In order to understand the growth mechanism, in situ optical emission spectrum (OES) was conducted to monitor the system directly. By collecting the optical signal derived from the corona discharge through an optical fiber, real-time relative concentration of reactive species in the system can be acquired (Figure S14, Supporting Information). **Figure 3**a shows a typical OES spectrum of our reaction system. Similar to other Argon (Ar) plasma, the emission wavelength between 700 and 900 nm can be assigned to atomic Ar lines due to 4p–4s transitions. Based on these Ar lines, the temperature of the plasma can be calculated at ≈6030 K (Figures S15 and Table S3, Supporting Information). CH (388.3 nm) can also be detected in the OES.[39] Strong plasma emissions of C_2 at about 516.4 nm with head peaks at 473.7 and 563.4 nm can also be detected due to the radiative decay of the $C^*_2(A^3\Pi g)$ state, which can be ascribed to $C + C + Ar \rightarrow C^*_2(A^3\Pi g) + Ar$.[40] The weak emission peak at about 656.2 nm can be attributed to H_α.

The relative intensity of each active species can be used to represent its concentration. The relative intensity (concentration) change of CH, C_2, H_α, and Ar versus time at a low CH_4 concentration of 1.0 vol% is presented in Figure 3b. It can be seen that the concentration of Ar decreases rapidly at first and then slows down, while the concentrations of CH and C_2 increase initially and then decrease. Note that when the concentration of radicals goes down to nearly zero, corona discharge will end. Moreover, the concentration of H_α remains almost the same throughout the process, indicating hydrogen ($CH_4 \rightarrow$ Graphene + $2H_2$) produced in the system is in the form of molecules. However, when increasing the concentration of methane from 1.0 to 13.0 vol%, the time of corona discharge decreases from over 200 s to seconds (Figure 3c,d; Figure S16a, Supporting Information). The maximal concentration of CH radicals remains nearly the same while the maximal concentration of C_2 radicals increases (Figure 3c,d). Considering the higher production rate of graphene in this case, it is assumed that C_2 radicals are more relevant to forming GS, consistent with previous work.[41]

The process of producing graphene is assumed to be the following

$$CH_4 \xrightarrow{k_1} CH \xrightarrow{k_2} C_2 \xrightarrow{k_3} \text{Graphene} \quad (1)$$

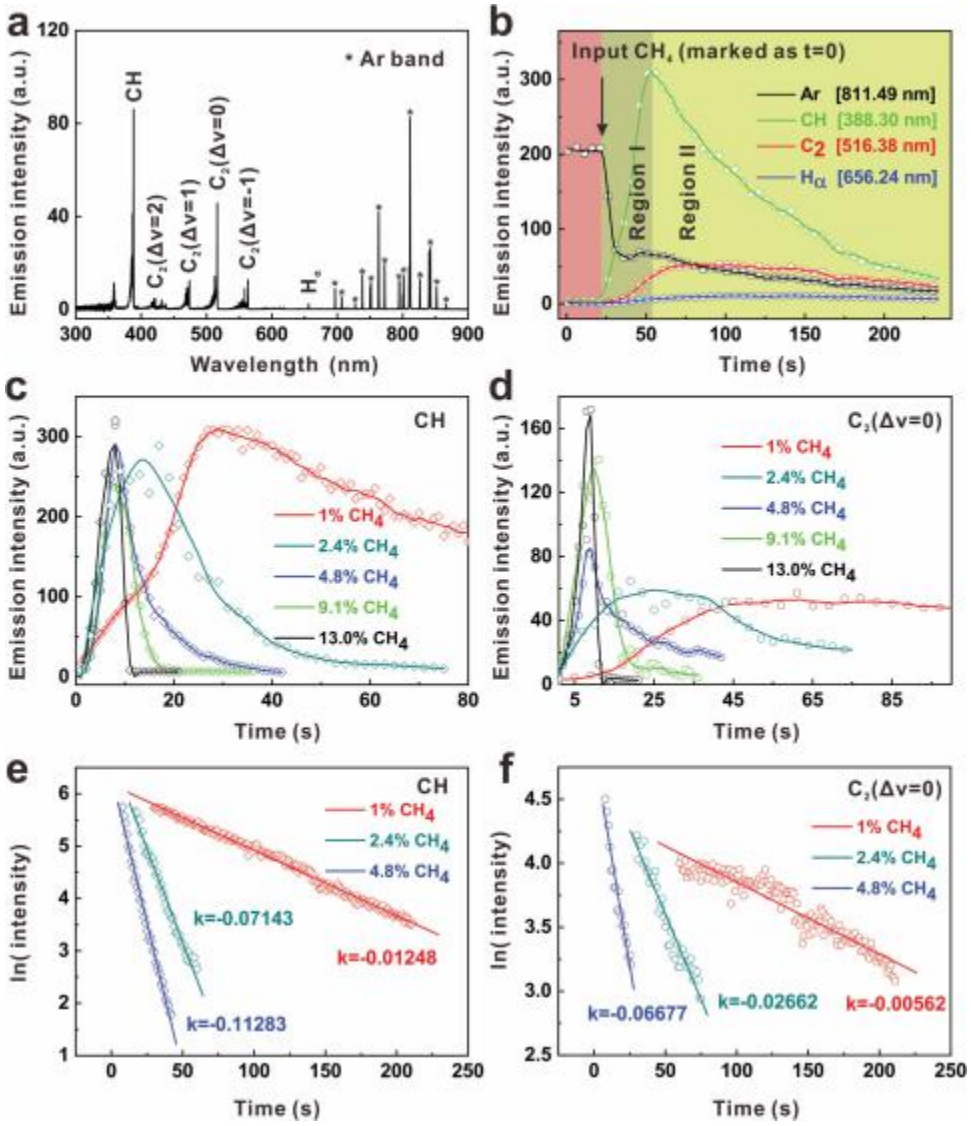

Figure 3. Mechanism of snowing GS during the corona discharge process. a) A typical in situ OES spectrum of the reaction system. b) Relative intensity change of CH, C_2, H_α, and Ar versus time at a low CH_4 concentration of 1.0 vol%. c,d) Relative intensity change of CH and C_2 ($\Delta v = 0$) radicals versus time at different concentration of CH_4. e,f) Plot of the logarithm of intensity of CH radicals and C_2 ($\Delta v = 0$) radicals versus time at different concentration of CH_4 during the period of decreasing concentration of radicals, indicating first-order reaction kinetics.

During the period of increasing concentration of radicals going up, in which radicals are generated faster than consumed ($k_1 > k_2 > k_3$), it can be seen that the concentrations of CH radicals and C_2 radicals increases linearly with time, following zero-order reaction kinetics (Figure S17, Supporting Information). Also, the net concentration of CH radicals increases faster than C_2 radicals indicates that $|k_1 - k_2| > |k_2 - k_3|$. Increasing the feed of methane will lead to a faster producing rate of CH radicals and C_2 radicals (Figure S17, Supporting Information), therefore it favors the accumulation of radicals. In the period of decreasing radical concentration, in which radicals are consumed faster than generated ($k_1 < k_2 < k_3$), it can be seen that the logarithms of concentration of Ar, CH radicals, and C_2 radicals decreases linearly with time, following first-order reaction kinetics (Figure 3e,f; Figure S16b, Supporting Information). The faster consumption rate of CH radicals compared to C_2 radicals indicates $|k_2 - k_1| > |k_3 - k_2|$, leading to an increase in relative concentration of C_2/CH (Figure S16c, Supporting Information). Increasing the feed of methane can lead to a faster consumption rate of CH radicals and C_2 radicals (Figure 3e,f), therefore a faster generation rate of GS, corresponding with Figure S13 in the Supporting Information. Thus, it is necessary to increase the feed of carbon sources in order to obtain a higher producing rate of graphene, but an associated larger concentration of C_2 will make it easier to form nucleation centers, so multilayer graphene will more likely be created at the same time.

It is also found that high quality GS can only be formed if the corona discharge is generated (Figure S18, Supporting Information), which might be attributed to the presence of

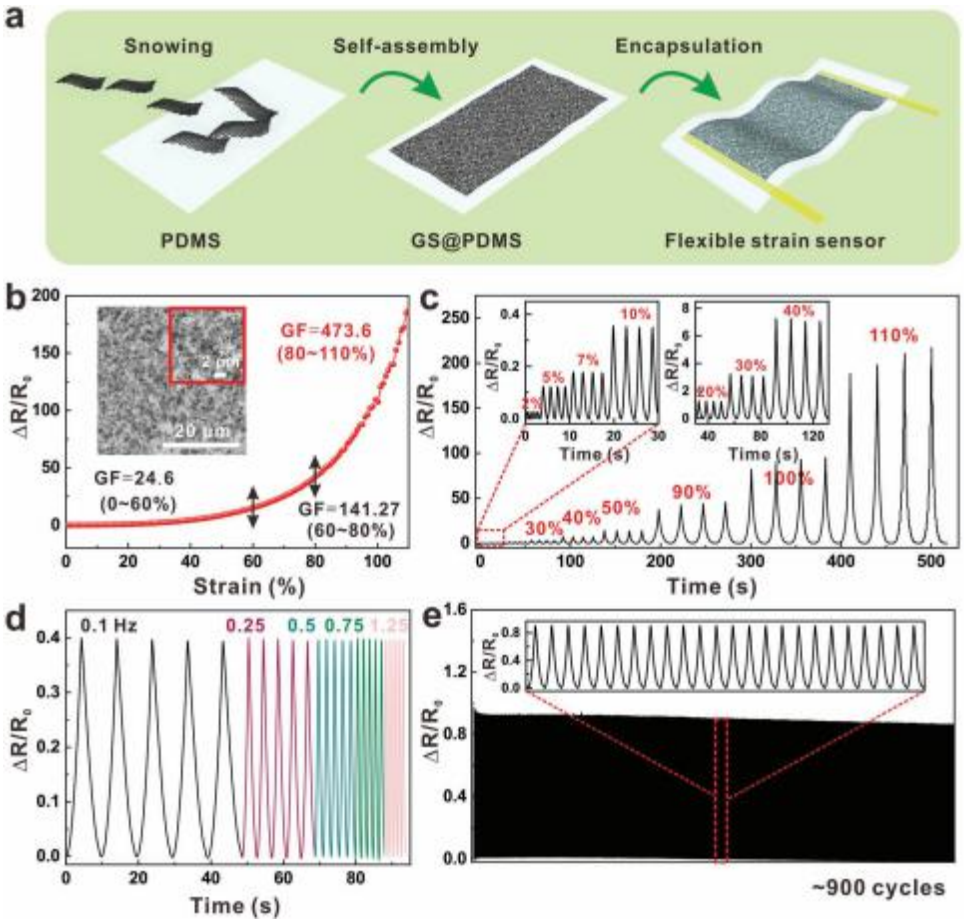

Figure 4. Electromechanical performance of GS based strain sensors. a) Scheme of snowing GS directly on PDMS film using microwave ovens to fabricate strain sensors. b) Plot of the relative change of resistance versus strain, showing a high GF as well as large workable strain range. SEM image (as an inset) shows that GS overlaps with each other to form a network structure. c) Relative change of resistance under varied strain, revealing reliable response to the applied strain. d) Relative change of resistance tested over a frequency range from 0.1 to 1.25 Hz. e) Cycling performance of the strain sensor at a loading applied strain of 20%, achieving long-time stability and high durability.

C_2. During this process, Ar plasma will collide with carbon sources causing bond fracture and formation of C_2 radicals, then formation of graphene. Note that the pyrolysis of methane will also contribute to the growth of graphene. However, the accumulation of H_2 in the system will suppress corona discharge as can be seen from the fact that discharge is significantly reduced when putting the same flow of hydrogen into the system (Figure S19, Supporting Information). The introduction of fresh Ar would generate corona discharge again (Figures S20a and S21, Supporting Information), because the energy needed to ionize H_2 molecules is much higher than CH_4. So, H_2 molecules, as by-products, will dilute the reaction system and suppress the corona discharge. Therefore, periodic influx of large amounts of Ar will favor continuous production of GS (Figure S20b,c, Supporting Information). In short, with the help of in situ OES, it can be confirmed that C_2 plays an important role in producing GS, and the concentration of CH and C_2 experiences an increase with zero-order reaction kinetics then a decrease with first-order kinetics during a period of snowing GS. Also, this snowing process of GS is triggered by corona discharge and periodic introduction of large amounts of Ar can make the snowing process continuous, available for scalable production of graphene flakes.

Like the self-assembly of snowflakes into fluffy snowfield, GS flakes from the microwave oven can snow directly onto polydimethylsiloxane (PDMS) substrate in the downstream, forming foam-like 3D and fluffy macroscopic architectures on PDMS due to π–π interactions and repulsion of negative charges on the surface of the GS flakes (**Figure 4**a). These macroscopic architectures can be utilized to fabricate a strain sensor, which is simple as well as avoiding the use of solvents. It can be seen that GS on PDMS becomes denser and denser with increased deposition time, forming a uniform and fluffy 3D assembled framework (Figure S22, Supporting Information). Scanning electron microscope (SEM) images of a cross-section of GS@PDMS show that GS overlaps with each other and forms a relatively uniform overall distribution (Figure S23, Supporting Information). As seen in Figure 4b, a monotonic increase in relative change of resistance ($\Delta R/R$) versus strain (ε) from 0% to 110% can be observed. The curve is nonlinear as can be ascribed to our sensor being a resistive-type strain sensor and microstructure in the strain sensor undergoes

"nonhomogeneous morphology" upon stretching, which is common in some previous works.[42] Generally speaking, gauge factor (GF), defined as $GF = (\Delta R/R)/\varepsilon$, can be used to measure its sensitivity. It can be seen that our strain sensor performs in three parts at 0%–60%, 60%–80%, and 80%–110%, with GFs of 24.6, 141.27, and 473.6, respectively, demonstrating its high sensitivity as well as large workable strain range. It should be mentioned that our sensor underwent rupture training with a rate of 1 mm s^{-1} before testing. Conventional strain sensors based on graphene exhibited either large workable range (1000%) but low gauge factor (2) or small workable range (6%) but high gauge factor (1000).[43,44] In contrast, our self-assembled stain sensor can realize a synergy of high sensitivity and large workable range, therefore giving superior performance to others![20,45] (Figure S24, Supporting Information).

In another experiment, spray coating process was employed to spray GS in solvents onto PDMS film. Compared with snowing GS directly on PDMS, the spray coating method can achieve denser packing of graphene but with lower GF. The reason can be ascribed to closer π–π stacking introduced by spraying graphene while more unstable contact points are generated by the snowing process (Figures S25 and S26, Supporting Information). In addition, our GS-based strain sensor shows stable and reliable response to applied strain. As seen in Figure 4c, the relative change of resistance increases with increasing applied strain, which can be as small as 2% or as large as 110%, corresponding well with Figure 4b. Almost, the same response of strain sensor can be achieved within the tested frequency range (0.1–1.25 Hz), exhibiting frequency independence (Figure 4d). In addition, the strain sensor can achieve long-time stability and high durability as the relative change of resistance remains nearly the same after 900 cycles at a loading applied strain of 20% (Figure 4e).

In order to unveil more details of the strain sensors when working, SEM images of a strain sensor at different loading strain was conducted. It can be seen that the crack gap increases with strain, which contributes to a high-performance strain sensor (Figure S27, Supporting Information). The GS-based strain sensor can also be used to simulate bending and touching. Different signals can be achieved by applying different forces to cause different deformation, demonstrating a possible application as wearable devices (Figure 5; Figure S28, Supporting Information).

Note that in addition to fluffy macroscopic architectures acquired by "snowing" GS, close stacking macroscopic architectures can be formed by printing GS. In our experiment, GS can be used as inks to fabricate patterned graphene electrodes. *N*-methyl pyrrolidone (NMP) is a good solvent to disperse GS and achieves high zeta potential (Figures S29 and S30, Supporting Information). GS can also be dispersed in ethanol/terpineol solution containing ethyecellulose (EC), and can achieve a concentration of 2 mg mL^{-1} for inkjet printing (Figure S31, Supporting Information). Traditional A4 paper, Silicon wafer, and polyimide (PI) are used to pattern GS, well comparable with commercial inks (Figures S32 and S33, Supporting Information). Besides, the patterned GS lines exhibit good electrical and mechanical properties, and can be applied to a keyboard (Figure S34, Supporting Information). All of these demonstrate the possibility of printing flexible circuits based on our GS.

We demonstrate a substrate-free and catalyst-free process for scalable preparation of "snowing" graphene flakes with high quality and low-cost. Utilizing corona discharge of SiO_2/Si in an ordinary household microwave oven at ambient pressure, large quantities of high quality GS can be generated by "snowing" directly in the gas phase. Notably, high yield and rate of graphene flakes production can be achieved in laboratory-scale apparatus. In situ OES confirms that C_2 plays an important role in producing graphene, and the concentration of CH and C_2 experiences an increase with zero-order reaction kinetics then a decrease with first-order kinetics during a period of corona discharge. GS can also self-assemble into foam-like, fluffy, 3D macroscopic architectures by directly "snowing" onto various substrates, exhibiting high sensitivity as well as large workable strain range when applied to strain sensors. Alternatively, close stacking macroscopic architectures of graphene patterns can be obtained by inkjet printing, showing good conductivity and mechanical properties. Not limited to producing graphene, we believe that the method we have described could also be extended to other 2D materials, and the way to assemble microscopic architectures into macroscopic architectures will be useful for various applications.

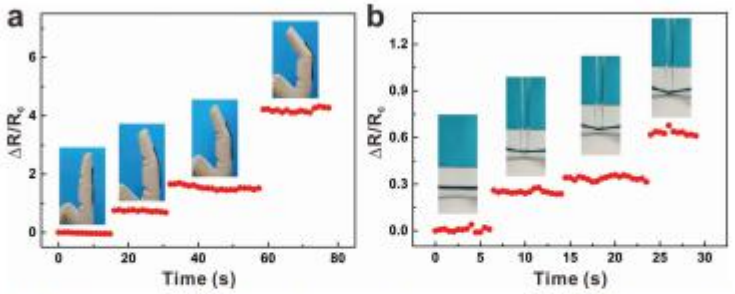

Figure 5. Detection of bending and touching using GS based strain sensors. Response to a) bending and b) touching by applying different forces to cause different deformation. Insets are the photographs of GS based strain sensors.

Experimental Section

Snowing Graphene using Microwave Ovens: A corona discharge process of growing graphene was adopted using a conventional household microwave oven with a frequency of 2.45 GHz and a power of 700 W. Three pieces of ≈1.5 × 2 × 0.05 cm^3 Si slice with 300 nm SiO_2 coating were put inside a quartz tube after cleaning. Note that the edges of SiO_2/Si were not smooth enough, some protuberance with small radius of curvature can serve as tips which can be used to trigger corona discharge. Argon (gas flow, 300–400 sccm) was brought into the tube to expel the residual air and then the tube was exposed to the microwave irradiation. A bright flash could be observed and then a nominal amount of methane (gas flow, 4–60 sccm) was brought into the tube at ambient pressure for seconds to minutes. After reaction, the tube was cooled naturally under the protection of argon. GS can be collected under the downstream or scraped off the wall.

Fabrication of GS-Based Strain Sensor: A polydimethylsiloxane (PDMS) film with thickness of ≈410 µm was put in the downstream at a distance of ≈25 cm from the Si slice. GS was deposited directly on the PDMS substrate (labeled as GS@PDMS). The GS@PDMS obtained was (i) cut into rectangular shapes, (ii) attached to copper wires at the two ends, and (iii) encapsulated by PDMS.

Characterization: The morphology and detailed structure of GS was investigated by SEM (Hitachi S-4800, Japan) at an accelerating voltage of 1.0 kV, TEM (FEI Tecnai F30; acceleration voltage 300 kV), aberration-corrected atomic-resolved TEM (Titan Cubed Themis G2 300; 80 kV). Raman spectroscopy (Horiba Jobin Yvon LabRAM HR 800, 514.5 nm), XPS (Kratos Analytical Axis-Ultra spectrometer with *Al Kα* X-ray source), and XRD (D/MAX-PC 2500; Cu $K_{\alpha1}$) were performed to investigate its quality. In situ OES (AvaSpec-ULS2048) was conducted to monitor the system in order to investigate the reaction mechanism. UV–vis spectroscopy (Perkin Elmer Lambda 950) was used to measure the transmittance of the GS based strain sensors. Electromechanical performance of the strain sensors was measured with a testing machine (Shimadzu AGS-X) and a digital source meter (Keithley 2400). TM990D Infrared Thermometer was used to monitor the temperature.

Supporting Information

Supporting Information is available from the Wiley Online Library or from the author.

Acknowledgements

The authors thank Dr. Ke Chen for his kind help in discussing the mechanism. The authors thank Jingwen Deng from Peking University for help and discussion on drawing the schematic diagram. The authors thank Prof. Yi Cheng from Tsinghua University for the kind instrument support of in situ OES. The authors thank Prof. Yanlin Song, Zhenkun Gu from Institute of Chemistry, Chinese Academy of Sciences for their help and discussion on inkjet printing of graphene. The authors thank Prof Jingmin Zhang and Chen Yin from Peking University for data collection of low-magnification and aberration-corrected atomic-resolved TEM image of graphene. This research was supported by Ministry of Science and Technology of China (2016YFA0200101 and 2016YFA0200104), the National Natural Science Foundation of China (Grant Nos. 51432002, 51720105003 and 21790052), and the Beijing Municipal Science and Technology Project (Grant No. Z161100002116026). Volunteers participated in the studies following informed consent.

Conflict of Interest

The authors declare no conflict of interest.

Keywords

corona discharge, macroscopic architectures, snowing graphene, strain sensors

Received: May 18, 2018
Revised: June 25, 2018
Published online: August 21, 2018

[1] A. K. Geim, K. S. Novoselov, *Nat. Mater.* **2007**, *6*, 183.
[2] K. S. Novoselov, V. I. Fal'ko, L. Colombo, P. R. Gellert, M. G. Schwab, K. Kim, *Nature* **2012**, *490*, 192.
[3] A. Zurutuza, C. Marinelli, *Nat. Nanotechnol.* **2014**, *9*, 730.
[4] W. S. Hummers, R. E. Offeman, *J. Am. Chem. Soc.* **1958**, *80*, 1339.
[5] Y. W. Zhu, S. Murali, W. W. Cai, X. S. Li, J. W. Suk, J. R. Potts, R. S. Ruoff, *Adv. Mater.* **2010**, *22*, 3906.
[6] J. K. Wassei, R. B. Kaner, *Acc. Chem. Res.* **2013**, *46*, 2244.
[7] M. J. Allen, V. C. Tung, R. B. Kaner, *Chem. Rev.* **2010**, *110*, 132.
[8] G. Eda, G. Fanchini, M. Chhowalla, *Nat. Nanotechnol.* **2008**, *3*, 270.
[9] Z. P. Chen, W. C. Ren, L. B. Gao, B. L. Liu, S. F. Pei, H. M. Cheng, *Nat. Mater.* **2011**, *10*, 424.
[10] S. F. Pei, Q. W. Wei, K. Huang, H. M. Cheng, W. C. Ren, *Nat. Commun.* **2018**, *9*, 9.
[11] Y. Hernandez, V. Nicolosi, M. Lotya, F. M. Blighe, Z. Y. Sun, S. De, I. T. McGovern, B. Holland, M. Byrne, Y. K. Gun'ko, J. J. Boland, P. Niraj, G. Duesberg, S. Krishnamurthy, R. Goodhue, J. Hutchison, V. Scardaci, A. C. Ferrari, J. N. Coleman, *Nat. Nanotechnol.* **2008**, *3*, 563.
[12] K. R. Paton, E. Varrla, C. Backes, R. J. Smith, U. Khan, A. O'Neill, C. Boland, M. Lotya, O. M. Istrate, P. King, T. Higgins, S. Barwich, P. May, P. Puczkarski, I. Ahmed, M. Moebius, H. Pettersson, E. Long, J. Coelho, S. E. O'Brien, E. K. McGuire, B. M. Sanchez, G. S. Duesberg, N. McEvoy, T. J. Pennycook, C. Downing, A. Crossley, V. Nicolosi, J. N. Coleman, *Nat. Mater.* **2014**, *13*, 624.
[13] K. S. Kim, Y. Zhao, H. Jang, S. Y. Lee, J. M. Kim, K. S. Kim, J. H. Ahn, P. Kim, J. Y. Choi, B. H. Hong, *Nature* **2009**, *457*, 706.
[14] S. Bae, H. Kim, Y. Lee, X. F. Xu, J. S. Park, Y. Zheng, J. Balakrishnan, T. Lei, H. R. Kim, Y. I. Song, Y. J. Kim, K. S. Kim, B. Ozyilmaz, J. H. Ahn, B. H. Hong, S. Iijima, *Nat. Nanotechnol.* **2010**, *5*, 574.
[15] X. S. Li, W. W. Cai, J. H. An, S. Kim, J. Nah, D. X. Yang, R. Piner, A. Velamakanni, I. Jung, E. Tutuc, S. K. Banerjee, L. Colombo, R. S. Ruoff, *Science* **2009**, *324*, 1312.
[16] A. Dato, V. Radmilovic, Z. Lee, J. Phillips, M. Frenklach, *Nano Lett.* **2008**, *8*, 2012.
[17] Y. Ando, X. Zhao, M. Ohkohchi, *Carbon* **1997**, *35*, 153.
[18] A. Dato, M. Frenklach, *New J. Phys.* **2010**, *12*, 24.
[19] K. S. Subrahmanyam, L. S. Panchakarla, A. Govindaraj, C. N. R. Rao, *J. Phys. Chem. C* **2009**, *113*, 4257.
[20] Y. R. Jeong, H. Park, S. W. Jin, S. Y. Hong, S. S. Lee, J. S. Ha, *Adv. Funct. Mater.* **2015**, *25*, 4228.
[21] E. Steven, W. R. Saleh, V. Lebedev, S. F. A. Acquah, V. Laukhin, R. G. Alamo, J. S. Brooks, *Nat. Commun.* **2013**, *4*, 8.
[22] X. Huang, X. Y. Qi, F. Boey, H. Zhang, *Chem. Soc. Rev.* **2012**, *41*, 666.
[23] Z. Li, Z. Liu, H. Y. Sun, C. Gao, *Chem. Rev.* **2015**, *115*, 7046.
[24] H. H. Cheng, Y. X. Huang, G. Q. Shi, L. Jiang, L. T. Qu, *Acc. Chem. Res.* **2017**, *50*, 1663.
[25] Z. Xu, C. Gao, *Acc. Chem. Res.* **2014**, *47*, 1267.
[26] D. A. Dikin, S. Stankovich, E. J. Zimney, R. D. Piner, G. H. B. Dommett, G. Evmenenko, S. T. Nguyen, R. S. Ruoff, *Nature* **2007**, *448*, 457.
[27] H. H. Cheng, Y. Hu, F. Zhao, Z. L. Dong, Y. H. Wang, N. Chen, Z. P. Zhang, L. T. Qu, *Adv. Mater.* **2014**, *26*, 2909.
[28] C. Li, G. Q. Shi, *Nanoscale* **2012**, *4*, 5549.
[29] Z. Bo, K. H. Yu, G. H. Lu, S. M. Cui, S. Mao, J. H. Chen, *Energy Environ. Sci.* **2011**, *4*, 2525.

[30] A. C. Ferrari, J. C. Meyer, V. Scardaci, C. Casiraghi, M. Lazzeri, F. Mauri, S. Piscanec, D. Jiang, K. S. Novoselov, S. Roth, A. K. Geim, *Phys. Rev. Lett.* **2006**, *97*, 4.
[31] K. H. Park, B. H. Kim, S. H. Song, J. Kwon, B. S. Kong, K. Kang, S. Jeon, *Nano Lett.* **2012**, *12*, 2871.
[32] W. Gao, L. B. Alemany, L. J. Ci, P. M. Ajayan, *Nat. Chem.* **2009**, *1*, 403.
[33] H. B. Feng, R. Cheng, X. Zhao, X. F. Duan, J. H. Li, *Nat. Commun.* **2013**, *4*, 7.
[34] Y. B. Chen, J. Y. Sun, J. F. Gao, F. Du, Q. Han, Y. F. Nie, Z. Chen, A. Bachmatiuk, M. K. Priydarshi, D. L. Ma, X. J. Song, X. S. Wu, C. Y. Xiong, M. H. Rummeli, F. Ding, Y. F. Zhang, Z. F. Liu, *Adv. Mater.* **2015**, *27*, 7839.
[35] X. C. Dong, H. Xu, X. W. Wang, Y. X. Huang, M. B. Chan-Park, H. Zhang, L. H. Wang, W. Huang, P. Chen, *ACS Nano* **2012**, *6*, 3206.
[36] K. Chen, C. Li, L. R. Shi, T. Gao, X. J. Song, A. Bachmatiuk, Z. Y. Zou, B. Deng, Q. Q. Ji, D. L. Ma, H. L. Peng, Z. L. Du, M. H. Rummeli, Y. F. Zhang, Z. F. Liu, *Nat. Commun.* **2016**, *7*, 9.
[37] I. K. Moon, J. Lee, R. S. Ruoff, H. Lee, *Nat. Commun.* **2010**, *1*, 6.
[38] D. Parviz, S. Das, H. S. T. Ahmed, F. Irin, S. Bhattacharia, M. J. Green, *ACS Nano* **2012**, *6*, 8857.
[39] H. B. Zhang, T. F. Cao, Y. Cheng, *Carbon* **2015**, *86*, 38.
[40] E. Tatarova, A. Dias, J. Henriques, A. M. B. do Rego, A. M. Ferraria, M. V. Abrashev, C. C. Luhrs, J. Phillips, F. M. Dias, C. M. Ferreira, *J. Phys. D. Appl. Phys.* **2014**, *47*, 11.
[41] Z. Qiu, P. Li, Z. Li, J. Yang, *Acc. Chem. Res.* **2018**, *51*, 728.
[42] M. Amjadi, K. U. Kyung, I. Park, M. Sitti, *Adv. Funct. Mater.* **2016**, *26*, 1678.
[43] C. S. Boland, U. Khan, C. Backes, A. O'Neill, J. McCauley, S. Duane, R. Shanker, Y. Liu, I. Jurewicz, A. B. Dalton, J. N. Coleman, *ACS Nano* **2014**, *8*, 8819.
[44] X. Li, R. J. Zhang, W. J. Yu, K. L. Wang, J. Q. Wei, D. H. Wu, A. Y. Cao, Z. H. Li, Y. Cheng, Q. S. Zheng, R. S. Ruoff, H. W. Zhu, *Sci. Rep.* **2012**, *2*, 6.
[45] Q. Liu, M. Zhang, L. Huang, Y. R. Li, J. Chen, C. Li, G. Q. Shi, *ACS Nano* **2015**, *9*, 12320.